ELSEVIER

Earth and Planetary Science Letters 174 (2000) 247–263

EPSL

www.elsevier.com/locate/epsl

Large volume recycling of oceanic lithosphere over short time scales: geochemical constraints from the Caribbean Large Igneous Province

F. Hauff [a,*], K. Hoernle [a], G. Tilton [b], D.W. Graham [c], A.C. Kerr [d]

[a] *GEOMAR Research Center, Wischhofstrasse 1–3, 24148 Kiel, Germany*
[b] *Department of Geology, University of California, Santa Barbara, CA 93106, USA*
[c] *College of Oceanography and Atmospheric Sciences, Oregon State University, Corvallis, OR 97331, USA*
[d] *Department of Geology, University of Leicester, University Road, Leicester LE1 7RH, UK*

Received 24 September 1998; accepted 27 October 1999

Abstract

Oceanic flood basalts are poorly understood, short-term expressions of highly increased heat flux and mass flow within the convecting mantle. The uniqueness of the Caribbean Large Igneous Province (CLIP, 92–74 Ma) with respect to other Cretaceous oceanic plateaus is its extensive sub-aerial exposures, providing an excellent basis to investigate the temporal and compositional relationships within a starting plume head. We present major element, trace element and initial Sr–Nd–Pb isotope composition of 40 extrusive rocks from the Caribbean Plateau, including onland sections in Costa Rica, Colombia and Curaçao as well as DSDP Sites in the Central Caribbean. Even though the lavas were erupted over an area of $\sim 3\times10^6$ km^2, the majority have strikingly uniform incompatible element patterns (La/Yb = 0.96 ± 0.16, $n = 64$ out of 79 samples, 2σ) and initial Nd–Pb isotopic compositions (e.g. $^{143}Nd/^{144}Nd_{in} = 0.51291 \pm 3$, $\varepsilon_{Ndi} = 7.3 \pm 0.6$, $^{206}Pb/^{204}Pb_{in} = 18.86 \pm 0.12$, $n = 54$ out of 66, 2σ). Lavas with endmember compositions have only been sampled at the DSDP Sites, Gorgona Island (Colombia) and the 65–60 Ma accreted Quepos and Osa igneous complexes (Costa Rica) of the subsequent hotspot track. Despite the relatively uniform composition of most lavas, linear correlations exist between isotope ratios and between isotope and highly incompatible trace element ratios. The Sr–Nd–Pb isotope and trace element signatures of the chemically enriched lavas are compatible with derivation from recycled oceanic crust, while the depleted lavas are derived from a highly residual source. This source could represent either oceanic lithospheric mantle left after ocean crust formation or gabbros with interlayered ultramafic cumulates of the lower oceanic crust. High $^3He/^4He$ in olivines of enriched picrites at Quepos are ~12 times higher than the atmospheric ratio suggesting that the enriched component may have once resided in the lower mantle. Evaluation of the Sm–Nd and U–Pb isotope systematics on isochron diagrams suggests that the age of separation of enriched and depleted components from the depleted MORB source mantle could have been ≤ 500 Ma before CLIP formation and interpreted to reflect the recycling time of the CLIP source. Mantle plume heads may provide a mechanism for transporting large volumes of possibly young recycled oceanic lithosphere residing in the lower mantle back into the shallow MORB source mantle. © 2000 Elsevier Science B.V. All rights reserved.

* Corresponding author. Tel.: +49-431-600-2125; Fax: +49-431-600-2924; E-mail: fhauff@geomar.de

0012-821X/00/$ – see front matter © 2000 Elsevier Science B.V. All rights reserved.
PII: S0012-821X(99)00272-1

Keywords: mantle plumes; flood basalts; trace elements; isotopes; geochemistry; Galapagos Rift; hot spots

1. Introduction

Oceanic plateaus are thought to form through rapid accumulation of extremely large volumes of melt resulting from the melting of starting plume heads associated with the initiation of mantle plumes [1]. Some models relate their formation to episodic instabilities at thermal boundary layers such as the core–mantle boundary. Based on analogue experiments, it has been proposed that starting plume heads may form by thermal entrainment of surrounding mantle and can flatten to disks, 2000 km in diameter, upon encountering the base of the overlying lithosphere [2]. More recently, however, numerical models have suggested that thermal entrainment may not be an important process in generating plume heads [3,4]. The mode of formation and internal structure of starting plume heads are not fully understood.

Oceanic flood basalt events are particularly important because their melts do not necessarily interact with the continental lithosphere and may thus provide a more pristine insight into the initial composition of long-lasting mantle plumes. The most recent pulse of oceanic flood basalt volcanism occurred during the Mid to Late Cretaceous [5] and generated several giant oceanic plateaus such as the Ontong Java, Manihiki and Kerguelen. Since these plateaus are largely submerged they are difficult to sample without drilling. The Caribbean plate and several accreted terranes in Western Colombia and Ecuador (Fig. 1) have been interpreted to represent the tectonized equivalent of a single Pacific oceanic plateau that may have been generated from the Galápagos starting plume head and that became tectonically inserted between North and South America after its formation (e.g. [1,6]). Due to accretion onto continental margins, uplift along subduction zones and transform faults, as well as continued convergence between North and South America, numerous plateau fragments are exposed at different structural levels along the margins of the Caribbean plate [7], while DSDP/ODP drilling has sampled the central portions of the plateau [8]. The large extent of subaerial exposure of the Caribbean Large Igneous Province (CLIP) in conjunction with available $^{40}Ar/^{39}Ar$ data (e.g. [9]) provide a unique opportunity to investigate the composition of a starting plume head. We present a comprehensive study of trace element and initial Sr–Nd–Pb isotope ratios of extrusive rocks from throughout the Caribbean plateau including sections from Costa Rica, Colombia and Curaçao as well as DSDP drill cores of Leg 15 (Fig. 1). This study suggests that some flood basalt events may enable large volume recycling of oceanic lithosphere over relatively short time scales, ≤ 0.5 Ga.

2. Geological background

Seismic studies of the Colombian and Venezuelan basins (Fig. 1) reveal that the oceanic crust in some places is 2–3 times as thick as normal oceanic crust (15–20 km compared to ~ 7 km) and has a seismic velocity structure similar to the Ontong Java plateau [10]. Nannofossils and $^{40}Ar/^{39}Ar$ ages suggest that the main pulse of volcanism forming the CLIP occurred primarily between 92 and 88 Ma but continued to ~ 74 Ma (e.g. [8,9,11]). Most plate tectonic reconstructions place the origin of the Caribbean Plateau at the present location of the Galápagos Islands [6,12]. Other models favor an intra-Caribbean origin [13]; however, radiolarites of equatorial Pacific faunal affinities in Puerto Rico and Haiti are older than the proposed opening of the Proto-Caribbean and thus require large-scale lateral transport into their present location [14], consistent with formation of the CLIP in the Eastern Pacific. Paleomagnetic data of igneous rocks in Central America [15] also indicate formation at equatorial latitudes, in agreement with the location of the Galápagos hotspot. Accreted terranes in Costa Rica and Panama are interpreted to record the Early and Mid Tertiary evolution of the Galápagos hotspot track [11,16]. A more detailed summary of the general geology and ages of the sampled localities

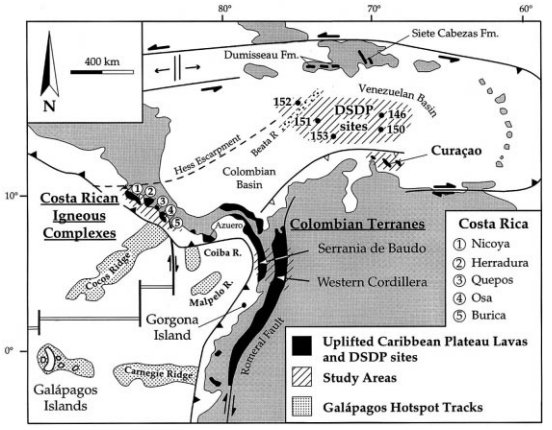

Fig. 1. Regional map of the Caribbean Large Igneous Province modified from [7,9].

in Colombia, Curaçao, Costa Rica and DSDP Leg 15 is found in Sinton et al. [9] and in the **EPSL Online Background Dataset**[1].

3. Analytical results

A description of the applied analytical methods is found in Appendix A. The **EPSL Online Background Dataset**[1] provides a reference list of literature data used as well as major and trace element data.

3.1. Major and trace elements

The extrusive rocks of the main plateau formation phase at ~90 Ma are primarily tholeiitic (Mg# = 45–65) and are hereafter referred to as CLIP tholeiites. Transitional tholeiites are relatively minor and occur at DSDP Site 151 and Gorgona Island and are referred to as CLIP E-basalts. Lavas of the subsequent hotspot track have tholeiitic (Osa) to transitional tholeiitic composition (Quepos). Previous studies (e.g. [7,8,11]) have emphasized that the vast majority of the CLIP tholeiites are related through fractional crystallization of olivine+plagioclase ± cpx ± Cr-spinel and that near primary melts like the Curaçao picrites (see **EPSL Online Background Dataset**[1]) are rarely sampled. Since some lavas have been affected by seawater alteration, the concentration of the most fluid mobile elements such as Rb, Ba, Sr, K and Na cannot always be taken as prime petrogenetic indicators, except for fresh glasses from the Nicoya peninsula or whole rocks with < 1.6 wt% loss on ignition (LOI) [11]. Therefore in many samples only the more immobile incompatible elements may reflect the original magmatic signature as shown in Fig. 2a, which summarizes all data. The most striking feature is the predominance of relatively flat patterns (62 samples) and the scarcity of lavas with enriched or depleted characteristics (DSDP Sites 151, 152). Among the lavas with flat patterns smaller variations are sometimes observed, for example $(La/Sm)_{N\ (\text{normalized to primitive mantle [17]})} = 0.78–1.06$ in the Curaçao lavas. Incompatible element patterns from Gorgona Island (**EPSL Online Background Dataset**, see footnote 1) and the younger Quepos ocean island and Osa terrane [11,18] are similar to those of Sites 151 and 152 and bracket the range of the CLIP basalts. Because all melts formed at relatively high degrees of partial melting, their incompatible element ratios approximate source ratios and thus the observed differences most likely reflect compositional variations in the source of the CLIP. Incompatible element patterns, including the fluid mobile elements of the freshest CLIP lavas, are shown in Fig. 2a. While the CLIP tholeiites have patterns similar to enriched (E-)MORB, the transitional tholeiites show similarities to ocean island basalt (OIB) end-member compositions at lower overall concentrations of the more incompatible elements (see [17,19]). The pattern of the freshest Gorgona komatiite is nearly identical to N-MORB, however, at significantly lower element concentrations which overlap with MORB gabbros [20]. Trace element ratios help to more clearly categorize the source character of the CLIP. On plots of La/Nb versus Zr/Nb (Fig. 2c) and Ba/Nb (not shown) the data spread along a linear array between N-MORB and HIMU (high time integrated $^{238}U/^{204}Pb$) OIB. Furthermore, the inverse correlation of La/Ce with the magnesium–iron ratio

[1] http://www.elsevier.nl/locate/epsl; mirror site: http://www.elsevier.com/locate/epsl

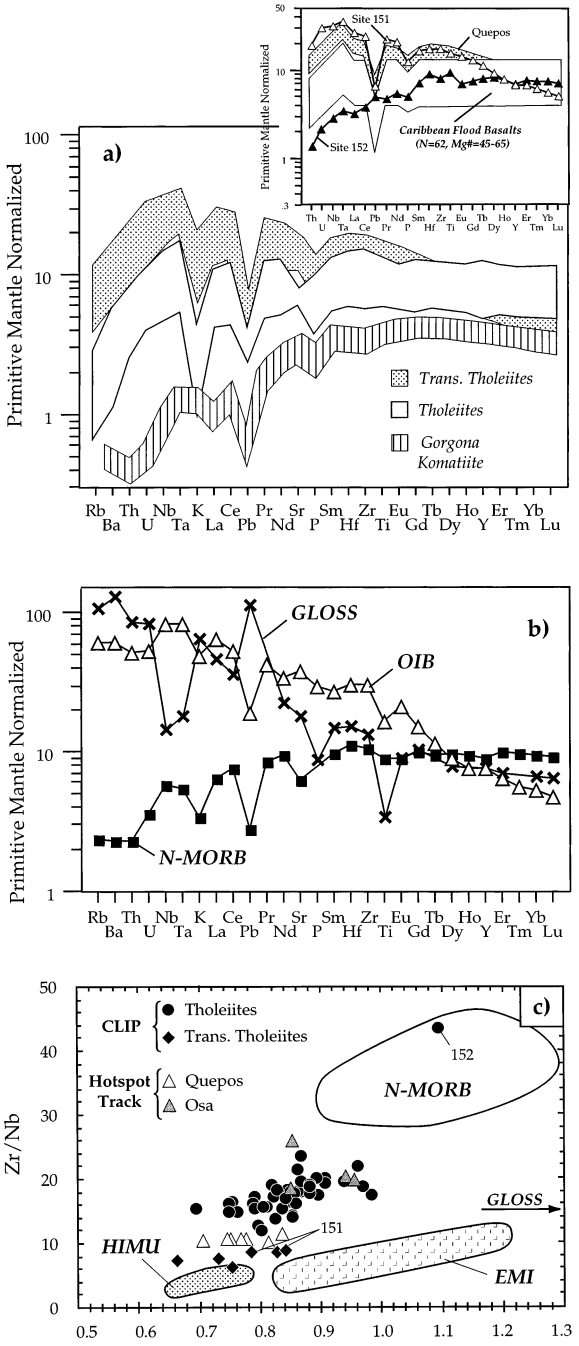

(not shown) indicates trace element and major element heterogeneities of the source.

3.2. Sr–Nd–Pb–He isotopes

In contrast to major and trace elements abundances, radiogenic isotope ratios are not fractionated by physical processes such as partial melting and fractional crystallization, and thus are commonly used as probes for the long-term chemical evolution of source regions. Nevertheless, the combined effects of alteration, crustal assimilation and radioactive decay can significantly change the initial isotopic composition of 75–92 Ma lavas necessitating careful data evaluation. Since seawater has relatively high Sr concentrations (8 ppm) and high $^{87}Sr/^{86}Sr$ (0.7075–0.7092 over the last ca. 90 Ma), it can significantly affect the magmatic $^{87}Sr/^{86}Sr$ signature of low-Sr (≤ 100 ppm) tholeiitic and picritic basalts. As shown in Fig. 3a, the initial Sr isotopic composition of unleached Caribbean Plateau lavas is highly variable ($(^{87}Sr/^{86}Sr)_{in} = 0.7031–0.7060$ at near constant $(^{143}Nd/^{144}Nd)_{in}$), consistent with seawater alteration. Since acid leaching is generally believed to reduce the effects of seawater alteration, leaching experiments (boiling in a mixture of 50% 6 N HCl and 50% 8 N HNO_3 for 3 h) were carried out on a subset of samples having the most radiogenic $(^{87}Sr/^{86}Sr)_{in}$ compositions on the unleached sample split. The effects of leaching from this and other studies (**EPSL Online Background Dataset**, see footnote 1) are displayed in Fig. 3a. Significant to moderate lowering of $^{87}Sr/^{86}Sr$ ratios after acid leaching is observed in samples that originate from coastal outcrops (e.g. Ser-

←

Fig. 2. (a) Generalized incompatible element diagram of the freshest CLIP basalts normalized to primitive mantle values of Hofmann [17]. Element patterns for the immobile incompatible elements are schematically shown for all CLIP in the inserted diagram. Additional data for Costa Rica and Gorgona island from [11] and the literature (**EPSL Online Background Dataset**, see footnote 1), [18]. (b) Reference incompatible element patterns for global subducted sediment (GLOSS [50]), average global OIB [19] and N-MORB [17]. (c) Zr/Nb versus La/Nb of the CLIP and subsequent hotspot track lavas. The fields for HIMU and EM I after Weaver [51].

rania de Baudó, Fig. 1) or DSDP drill cores. In a few samples $^{87}Sr/^{86}Sr$ remained unusually high ($^{87}Sr/^{86}Sr)_{in} = 0.7050–0.7064$) or even increased (sample CUR42). Either acid leaching is not always effective at removing Sr from secondary sources, when for example albitized feldspar is present [21], which is the case in the groundmass of several CLIP lavas, or the radiogenic Sr comes from a magmatic component, e.g. assimilated seawater or altered crust as suggested for the Curaçao lavas [22]. In either case, the measured $^{87}Sr/^{86}Sr$ ratios are believed to represent maximum source ratios.

In contrast to the Sr isotope system, the Nd isotope system is not significantly affected by seafloor alteration and metamorphism [20]. The vast majority of Caribbean lavas define a relatively narrow range of $(^{143}Nd/^{144}Nd)_{in} = 0.51291 \pm 3$. Exceptions are noted for the enriched lavas from DSDP Site 151 ($(^{143}Nd/^{144}Nd)_{in} = 0.51279$) and the depleted lavas from DSDP Site 152 ($(^{143}Nd/^{144}Nd)_{in} = 0.51304$). In addition the Curaçao picrites have lower $(^{143}Nd/^{144}Nd)_{in} = 0.51284$ than associated basalts (0.51285–0.51297). Among the Colombian terranes, there is a tendency from less radiogenic Nd ($(^{143}Nd/^{144}Nd)_{in} = 0.51289 \pm 3$) in the ~90 Ma lavas of the Western Cordillera towards more radiogenic Nd compositions ($(^{143}Nd/^{144}Nd)_{in} = 0.51294 \pm 1$) in the ~75 Ma Serranía de Baudó basalts. The Nd isotope ratios of most CLIP basalts are less radiogenic than Pacific N-MORB at 90 Ma [23], consistent with the involvement of enriched OIB mantle. However, the relatively radiogenic Nd composition is distinct from enriched (EM)-type OIB ($^{143}Nd/^{144}Nd < 0.5126$) but resembles HIMU-type OIB ($^{143}Nd/^{144}Nd = 0.5129$). Furthermore, the positive $\varepsilon_{Ndi} = 7.3 \pm 0.6$ indicates derivation from a long-term depleted source. Leached and unleached samples with $(^{87}Sr/^{86}Sr) < 0.7038$ show a crude negative correlation with $(^{143}Nd/^{144}Nd)_{in}$ that overlaps with the estimated Galápagos field at 90 Ma (Fig. 3a).

In contrast to the longer half-lives of ^{87}Rb ($t_{1/2} = 48 \times 10^9$ yr) and ^{147}Sm ($t_{1/2} = 106 \times 10^9$ yr), the shorter half-lives of ^{235}U ($t_{1/2} = 0.71 \times 10^9$ yr), ^{238}U ($t_{1/2} = 4.47 \times 10^9$ yr) and ^{232}Th ($t_{1/2} = 14 \times 10^9$ yr) and the relatively high parent/daughter ratios determined in some of the samples (e.g. $^{238}U/^{204}Pb = 3–71$) necessitate correction for radioactive decay in Cretaceous samples. An additional problem concerns the mobility of U (when oxidized as U^{6+}) and Pb during hydrothermal alteration in contrast to the relatively immobile behavior of Th (e.g. [20,24]). In this study we determined Pb isotope ratios and U–Th–Pb concentrations by isotope dilution on single dissolutions of the

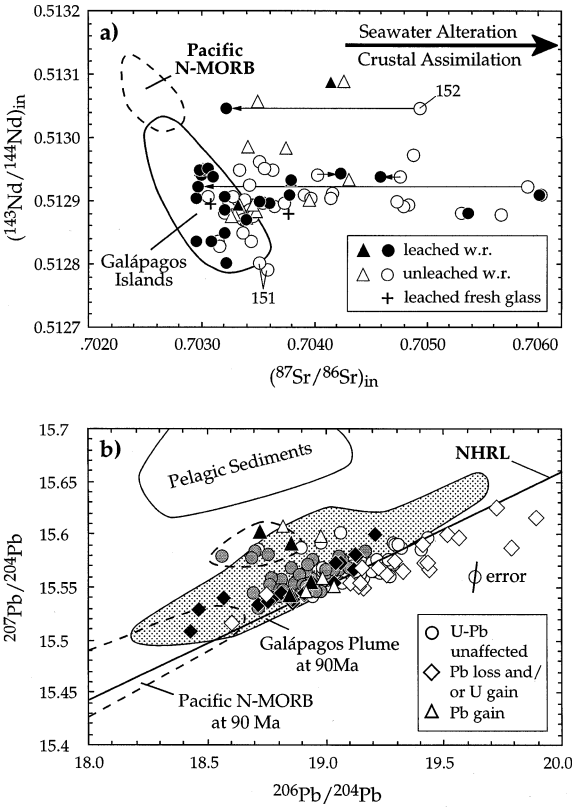

Fig. 3. (a) Initial Sr–Nd isotope ratios for unleached and leached samples: CLIP lavas (circles), hotspot track lavas (triangles). Initial Sr–Nd data for Galápagos and Pacific N-MORB were calculated using data from [23,32]. (b) Measured (open symbols) and initial (closed and shaded symbols) Pb isotope ratios of CLIP lavas. Lavas with high measured radiogenic $^{206}Pb/^{204}Pb$ correspond to samples with high μ values. Galápagos Pb isotope data from White et al. [32]. Due to a lack of U, Th, Pb concentration for Galápagos data, we assume a linear increase of μ with $^{206}Pb/^{204}Pb$ ($\mu = 10 \times ^{206}Pb/^{204}Pb - 175$ and $^{232}Th/^{238}U = 3$) in calculating the field for the Galápagos source, based on a comparison with similar rock types on Gran Canaria [52]. For additional data sources used in these plots see Fig. 2.

unleached sample, since hydrothermal alteration is likely to occur shortly after lava emplacement (see below). Leaching experiments on these samples revealed that U–Th–Pb are often strongly fractionated during acid leaching which significantly overestimates the correction for radioactive decay. For example μ in the unleached DSDP sample 153-1 is 14.7 while after cold leaching in 3 N HNO_3 μ increased to 40.5 [18]. Postmagmatic open system behavior can be tested by interelement correlation of U–Th–Pb with immobile elements such as Ce and Nd. Although U and Th correlate well for most samples (Th/U = 3.05, $R^2 = 0.99$, $n = 64$ out of 71), it is clear that a few samples have gained U (Fig. 4a). If Nd and Pb have similar distribution coefficients in dry mantle, then Nd/Pb is expected to be relatively constant in the oceanic mantle (24 ± 5) [25]. Accepting this assumption and that Nd is less fluid mobile than Pb during hydrothermal alteration [20], we use a plot of Pb versus Nd/Pb to identify samples that have either gained or lost Pb (Fig. 4b). Most CLIP samples have similar Nd/Pb as observed in MORB [25], but some show evidence of Pb mobility as part of their geochemical evolution, which most likely reflects hydrothermal alteration associated with the flood basalt event and thus occurred shortly after eruption. In this respect the large volume of rapidly erupted lava is likely to initiate extensive hydrothermal systems which are likely to influence ocean chemistry. Moreover, since secondary processes are capable of modifying ratios of incompatible elements with similar partition coefficients in dry mantle systems (e.g. Nd/Pb, Ce/Pb, Nb/U) they may also influence the long-term geochemical evolution of the continental crust and mantle depending on whether oceanic plateaus become accreted or subducted.

As shown in Fig. 3b and Table 1, correction for radioactive decay reduces the large spread of measured Pb isotope ratios (e.g. $(^{206}Pb/^{204}Pb)_m = 18.6–19.9$, $(^{208}Pb/^{204}Pb)_m = 38.3–39.9$) to a significantly narrower initial range ($(^{206}Pb/^{204}Pb)_{in} = 18.4–19.2$, $(^{208}Pb/^{204}Pb)_{in} = 38.0–38.8$). The samples with very radiogenic Pb have extreme μ of 40–70 due to U gain and/or Pb loss and thus their present Pb isotopic composition

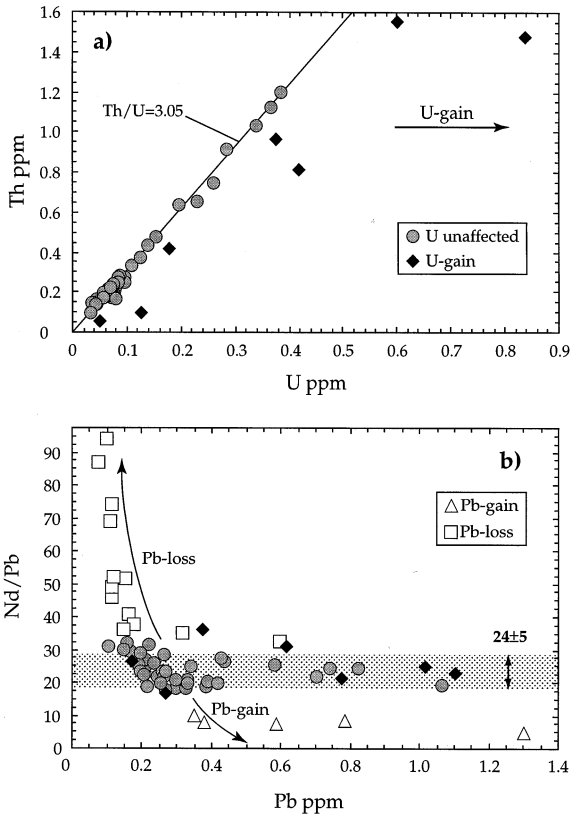

Fig. 4. Diagrams of (a) U vs. Th and (b) Pb vs. Nd/Pb illustrate the effects of seawater alteration/metamorphism on U and Pb concentrations. (a) Most samples have reasonably constant Th/U = 3.05, excluding samples: 152-2, 151-1, 151-2, AQ8, AQ72, OS6, AN46 appear to have gained U. It is assumed that Th is not affected by seawater alteration/metamorphism. (b) The majority of CLIP samples (gray circles) have Nd/Pb ratios similar to what is observed in MORB (24 ± 5 [25]) and thus their Pb concentrations have presumably not been significantly affected by hydrothermal alteration. The μ values in these samples range from 10 to 30. Samples AQ22, GO1, BN17, AN46, OS16, SDB8, -16, -18, -20, CUR32, -36, -42 (open squares) are believed to have experienced some Pb loss and samples SDB13, CUR8, AH8, PAN6 and 152-1 may have gained Pb (open triangles). Solid diamonds indicate U gain. Most samples with Pb loss or U gain have higher μ values (30–72) while samples with Pb gain have lowered μ values, < 8. U–Th–Pb concentrations were determined by TIMS–ID and Nd by ICP–MS. For additional Costa Rican data sources see Fig. 2.

mainly reflects radiogenic ingrowth rather than a primary source signature. The majority of Caribbean lavas evolved with moderate μ (10–30), which are still higher than observed in fresh tho-

Table 1
Observed and initial Sr–Nd–Pb isotope ratios of basalts from the CLIP

Sample	Age (Ma)	Rb[a] (ppm)	Sr[b] (ppm)	$^{87}Sr/^{86}Sr_{rm}$ unleached	$^{87}Sr/^{86}Sr_{rm}$ leached[c]	$^{87}Sr/^{86}Sr_{in}$	Sm[a] (ppm)	Nd[a] (ppm)	$^{147}Sm/^{144}Nd$	$^{143}Nd/^{144}Nd_{m.}$	$^{143}Nd/^{144}Nd_{in.}$	εNd_t	U[d] (ppm)	Th[d] (ppm)	Pb[d] (ppm)	$^{206}Pb/^{204}Pb_{m.}$	$^{207}Pb/^{204}Pb_{m.}$	$^{208}Pb/^{204}Pb_{m.}$	$^{206}Pb/^{204}Pb_{in.}$	$^{207}Pb/^{204}Pb_{in.}$	$^{208}Pb/^{204}Pb_{in.}$
Costa Rica: Nicoya																					
AN-046	90	1.44	109	0.703280 (7)		0.703231	4.54	13.50	0.202	0.513020 (8)	0.512901	7.39	0.180	0.414	0.376	19.150 (4)	15.553 (5)	38.682 (9)	18.718	15.532	38.356
AN-086	90	1.55	102	0.703484 (7)		0.703428	5.12	15.16	0.203	0.513012 (4)	0.512892	7.22	0.196	0.635	0.705	19.213 (2)	15.564 (3)	38.787 (5)	18.960	15.552	38.519
Costa Rica: Quepos																					
AQ8	60	4.64	264	0.703380 (8)		0.703337	5.19	18.95	0.165	0.512956 (4)	0.512891	6.45	0.379	0.964	0.616	19.417 (2)	15.590 (2)	39.012 (5)	19.044	15.573	38.700
AQ16	60	2.74	218	0.703523 (9)		0.703492	3.99	14.62	0.164	0.512945 (5)	0.512881	6.24	0.261	0.737	0.585	19.438 (2)	15.596 (3)	39.081 (6)	19.168	15.583	38.830
Curaçao																					
CUR8	90	1.33	46	0.703554 (12)		0.703447	0.95	2.93	0.195	0.512950 (5)	0.512835	6.11	0.042	0.133	0.382	18.820 (1)	15.607 (2)	38.284 (3)	18.722	15.602	38.182
CUR14	90	1.25	46	0.703250 (7)		0.703150	1.08	3.31	0.197	0.512951 (9)	0.512835	6.11	0.045	0.136	0.108	19.307 (2)	15.590 (3)	38.900 (8)	18.926	15.571	38.523
CUR20	90	0.14	69	0.703379 (7)		0.703371	1.47	4.51	0.196	0.512962 (4)	0.512847	6.33	0.058	0.189	0.197	19.075 (5)	15.553 (6)	38.820 (11)	18.809	15.541	38.535
CUR21	90	4.45	93	0.703541 (8)		0.703364	1.51	4.53	0.200	0.512986 (8)	0.512868	6.75	0.063	0.183	0.152	19.198 (4)	15.565 (4)	38.965 (9)	18.819	15.547	38.607
CUR32	90	5.68	175	0.705432 (8)	0.705500 (6)	0.705380	2.03	5.72	0.214	0.513004 (7)	0.512878	6.95	0.066	0.208	0.118	19.728 (6)	15.624 (7)	39.379 (14)	19.214	15.599	38.845
CUR33	90	1.28	84	0.703791 (8)	0.703658 (8)	0.703602	1.60	4.60	0.209	0.513019 (8)	0.512896	7.29	0.045	0.146	0.209	19.197 (5)	15.572 (6)	38.783 (11)	19.004	15.563	38.576
CUR36	90	0.65	103	0.704758 (8)	0.703548 (5)	0.703525	2.11	6.13	0.207	0.513019 (6)	0.512897	7.32	0.075	0.237	0.119	19.334 (6)	15.564 (7)	39.049 (15)	18.757	15.537	38.452
CUR42	90	1.77	258	0.704919 (8)	0.706705 (8)	0.706680	1.81	5.26	0.207	0.513094 (13)	0.512972	8.77	0.057	0.165	0.147	19.263 (4)	15.561 (5)	38.930 (10)	18.912	15.544	38.598
DSDP Leg15																					
146-1	90	0.35	124	0.704043 (9)	0.703019 (6)	0.703009	2.12	6.14	0.208	0.513061 (6)	0.512939	8.12	0.074	0.172	0.300	18.982 (2)	15.591 (2)	38.549 (4)	18.761	15.580	38.380
150-1	90	1.08	117	0.703580 (8)		0.703546	2.32	6.94	0.201	0.513012 (5)	0.512893	7.24	0.089	0.240	0.221	19.069 (2)	15.600 (2)	38.703 (4)	18.704	15.583	38.381
151-1	90	22.10	331	0.703843 (8)		0.703596	6.54	25.11	0.157	0.512883 (5)	0.512791	5.24	0.839	1.473	1.018	19.892 (1)	15.615 (1)	39.290 (2)	19.133	15.578	38.852
151-2	90	29.92	307	0.703876 (10)[e]	0.703469 (11)	0.703222	6.35	24.90	0.154	0.512890 (4)	0.512800	5.41	0.60[a]	1.55[a]	1.10[a]	19.567 (1)	15.596 (1)	39.184 (2)	19.068	15.572	38.763
152-1	75	12.26	114	0.705280 (8)	0.703551 (11)	0.703220	2.76	6.46	0.257	0.513170 (6)	0.513044	9.80	0.127	0.092	0.789	18.983 (3)	15.597 (3)	38.354 (7)	18.855	15.591	38.323
153-1	90	0.31	123	0.703978 (9)	0.702971 (10)	0.702961	2.88	8.15	0.213	0.513027 (6)	0.512902	7.40	0.097	0.242	0.422	18.898 (2)	15.587 (2)	38.518 (5)	18.692	15.577	38.349
Colombia: Western Cordillera																					
VIJ1	90	0.42	89	0.703445 (8)		0.703428	3.99	11.65	0.206	0.513005 (5)	0.512884	7.05	0.089	0.278	0.441	19.222 (2)	15.575 (3)	38.908 (6)	19.039	15.567	38.720
BAR5	90	0.74	99	0.703233 (8)		0.703205	1.78	5.73	0.187	0.512989 (4)	0.512879	6.96	0.085	0.270	0.266	19.276 (3)	15.560 4)	38.985 (9)	18.986	15.546	38.683
BAR7	90	1.04	417	0.703199 (6)		0.703157	1.91	6.15	0.187	0.512937 (17)	0.512827	5.94	0.085	0.240	0.238	19.349 (3)	15.604 (4)	39.155 (9)	19.007	15.566	38.776
CBU4	90	5.84	207		0.703884 (7)	0.703780	2.22	6.55	0.204	0.513027 (7)	0.512907	7.51	0.062	0.184	0.335	19.271 (3)	15.575 (3)	38.927 (7)	19.102	15.567	38.764
CBU12	90	2.71	33		0.704903 (6)	0.704599	3.99	11.78	0.175	0.513040 (9)	0.512937	8.10	0.139	0.431	0.432	19.197 (5)	15.565 (2)	38.820 (5)	18.906	15.551	38.523
CBU14	90	2.68	99	0.703292 (9)		0.703202	2.23	6.32	0.190	0.513018 (8)	0.512906	7.49	0.068	0.206	0.272	18.945 (3)	15.541 (3)	38.529 (7)	18.719	15.530	38.305
PAN6	90	1.04	91	0.703496 (6)		0.703454	2.18	6.29	0.208	0.512995 (3)	0.512872	6.83	0.071	0.218	1.302	18.987 (2)	15.557 (2)	38.631 (4)	18.938	15.555	38.582
Colombia: Serranía de Baudó																					
SDB5	75	2.73	184	0.703848 (9)	0.703847 (6)	0.703801	1.96	5.72	0.206	0.513033 (7)	0.512932	7.62	0.060	0.175	0.198	19.150 (4)	15.561 (5)	38.760 (11)	18.922	15.551	38.541
SDB8	75	0.80	228	0.703355 (8)		0.703344	2.69	7.68	0.211	0.513051 (9)	0.512948	7.92	0.077	0.227	0.112	19.440 (6)	15.567 (7)	39.001 (14)	18.916	15.542	38.497
SDB11	75	4.38	106		0.704364 (8)	0.704237	1.76	5.05	0.210	0.513046 (10)	0.512943	7.83	0.062	0.196	0.256	19.143 (3)	15.554 (3)	38.804 (7)	18.960	15.545	38.614
SDB13	75	0.85	91	0.703662 (9)		0.703633	1.24	3.46	0.216	0.513054 (5)	0.512948	7.93	0.033	0.093	0.353	18.918 (4)	15.545 (5)	38.480 (11)	18.848	15.542	38.415
SDB16	75	1.49	129	0.703593 (8)		0.703557	2.34	6.67	0.211	0.513054 (8)	0.512950	7.97	0.065	0.185	0.165	19.163 (3)	15.549 (3)	38.681 (7)	18.865	15.535	38.404
SDB18	75	1.23	156	0.704788 (8)	0.703131 (7)	0.703107	2.79	7.92	0.212	0.513040 (7)	0.512936	7.70	0.057	0.196	0.155	19.145 (6)	15.550 (6)	38.774 (15)	18.867	15.537	38.461
SDB20	75	2.16	112	0.705972 (8)	0.703032 (8)	0.702972	2.38	6.71	0.214	0.513027 (9)	0.512922	7.43	0.060	0.184	0.179	19.108 (4)	15.553 (5)	38.686 (11)	18.857	15.541	38.432
SDB21	75	6.11	306	0.706078 (8)	0.706069 (6)	0.706007	1.86	5.36	0.208	0.513009 (4)	0.512907	7.13	0.062	0.176	0.118	19.437 (3)	15.572 (3)	38.962 (7)	19.036	15.553	38.592

[a]ICP–MS, [b]XRF, [c]in 50% 6 N HCl and 50% 8 N HNO_3 for 3 h, [d]TIMS–ID.
Errors refer to the least significant digit and are 2σ mean within run precision. The normalization procedure of the isotopic data, isotopic standards, analytical precision and accuracy are given in the Appendix.

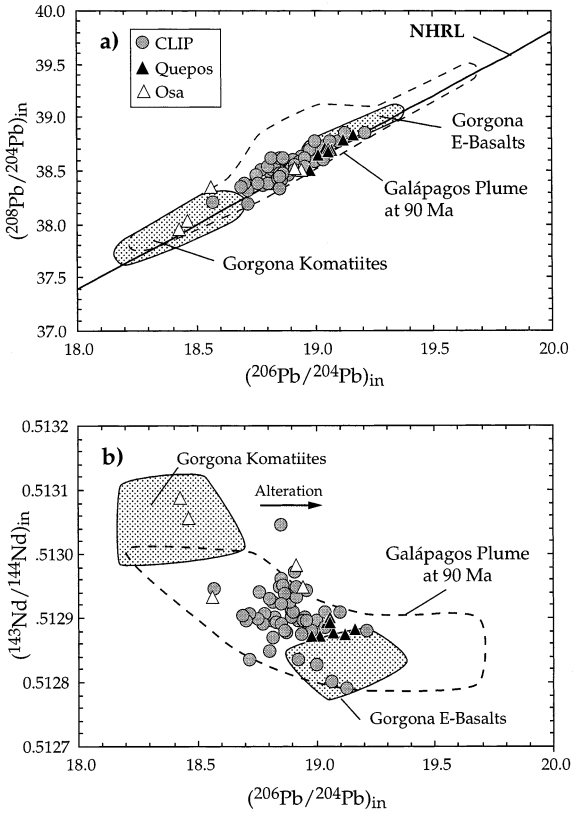

Fig. 5. Initial $^{206}Pb/^{204}Pb$ for CLIP basalts correlates (a) positively with initial $^{208}Pb/^{204}Pb$ and (b) negatively with initial $^{143}Nd/^{144}Nd$. Fields for Gorgona E-basalts and komatiites and the Galápagos Islands are from the literature (**EPSL Online Background Dataset**, see footnote 1). Since U–Th–Pb concentration data are not available on the same komatiite samples analyzed for isotopes except for one sample [53], we use $\mu = 6$, $^{232}Th/^{204}Pb$ $(\Omega) = 21$ for the remaining komatiites and $\mu = 30$, $\Omega = 100$ for the E-basalts, calculated from available U, Th, Pb concentration data [34,53]. See Fig. 2 for additional Costa Rican data sources.

leiitic MORB glasses (10 ± 5 [26]), but are characteristic for altered oceanic crust [20] and OIB. Despite mobilization of U and Pb, the vast majority of samples affected by alteration show similar initial Pb isotopic ratios to samples whose U and Pb were not affected, consistent with the disturbance of the U–Pb systematics shortly after eruption. Although U–Pb in the two least radiogenic samples are also affected, their μ values (19–31) are similar to the other samples not significantly affected by alteration, providing support for the idea that their initial Pb isotopic ratios are magmatic. Elevated $^{207}Pb/^{204}Pb$ ratios in some samples (CUR8, CUR32, OS9 and all DSDP samples) even after leaching in 3 N HNO_3 either indicates contamination with a crustal or seawater component through hydrothermal alteration [20,27] or may reflect a source characteristic. Since only two out of five samples which may show Pb gain (Fig. 4b) also have elevated $^{207}Pb/^{204}Pb$ ratios, possible Pb uptake need not necessarily coincide with crustal contamination. The variable U/Th ratios and elevated initial $^{207}Pb/^{204}Pb$ composition of the Leg 15 samples suggest that the uppermost plateau lavas were most severely affected by seawater alteration/metamorphism. In summary, the initial Pb isotope data are more radiogenic than Pacific MORB corrected to 90 Ma, plot as a group slightly above the Northern Hemisphere Reference Line (NHRL [28]) and completely fall within the range of the Galápagos Islands estimated at 90 Ma (Figs. 3b and 5).

Very fresh olivine separates of two Quepos picrites gave nearly identical high initial $^{3}He/^{4}He$ (11.4 and 11.7 ± 0.3 R/R_A (R_A being the atmospheric ratio of 1.39×10^{-6}) and He concentrations of $\sim 5.7 \times 10^{-9}$ cc STP/g. The He isotope ratios are considerably higher than observed in MORB (7–9 R/R_A) and endmember HIMU-type OIB from Santa Helena, Tubuaii and Mangaia but are within the range for the Galápagos Islands (7–23 R/R_A [29]).

4. Discussion

4.1. The Galápagos connection

The oldest structures of the Galápagos hotspot tracks presently being subducted off the coast of Ecuador and Costa Rica are ca. 15 Ma [30]. There are indications that the Cocos Ridge has been subducting beneath Costa Rica for at least 5 Ma, leaving a temporal gap of ca. 40 Ma in total between the present Galápagos tracks and the accreted Quepos and Osa terranes, which are interpreted as parts of the early Galápagos hotspot

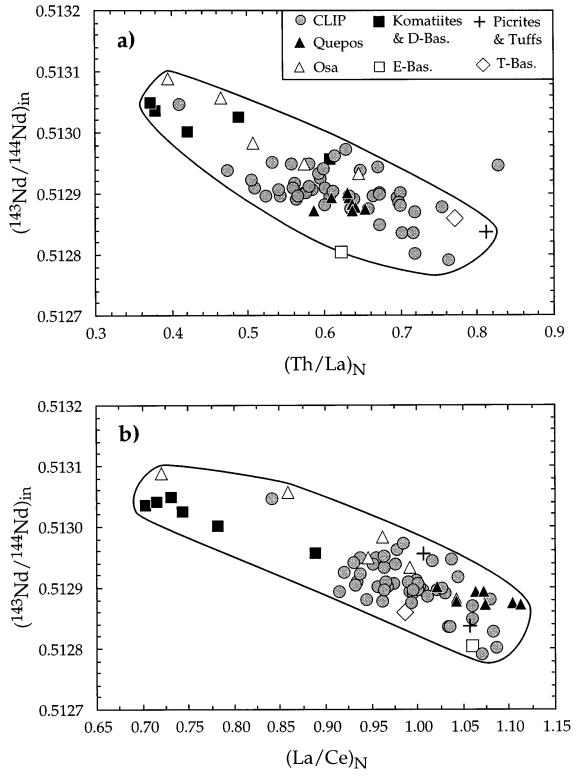

Fig. 6. Correlation of initial Nd isotope ratios with ratios of highly incompatible immobile elements normalized to primitive mantle [17]: (a) Th/La, (b) La/Ce. Gorgona data taken from the literature (**EPSL Online Background Dataset**, see footnote 1). Tuff sample GOR132 with very unradiogenic Nd and D-basalt GOR 94-12 [34] with a difference of 0.00008 for replicate Nd isotope analyses were excluded due to suspected crustal contamination.

track [11,18]. The spatial distribution of the Quepos and Osa terranes and the interpretation of their paleoenvironment are very similar to the Cocos aseismic ridge and seamounts (drowned ocean islands), presently being subducted off the coast of Costa Rica [30]. Nevertheless, the ca. 40 Ma gap in the history of the Galápagos hotspot is a serious problem in relating the Galápagos plume to the CLIP. On the other hand, studies of accreted ocean island and seamount complexes in southern Costa Rica and western Panama appear to record the Early and Mid Tertiary history of the Galápagos hotspot track ([16] and Hauff et al., in preparation), strengthening the link of the CLIP to the Galápagos hotspot. However, the extensive overlap of the CLIP Sr–Nd–Pb isotope data with the field determined for the Galápagos at 90 Ma (Figs. 3 and 5) cannot be taken as unique proof for derivation from the same plume since the large isotopic array of the present Galápagos Islands may largely result from interaction of the Galápagos plume with the Galápagos spreading center (e.g. [31,32]). On the other hand, high ^{3}He signatures in the Quepos picrites further support a link to the Galápagos hotspot, since it is one of the few high ^{3}He hotspots [29]. Finally we note that some hotspots linked to flood basalt events such as the Iceland plume are characterized by high ^{3}He (e.g. [33]). Nonetheless, an unequivocal link between the Galápagos hotspot and the CLIP will only be established if the history of the hotspot between 20 and 60 Ma can be reconstructed.

4.2. *Source heterogeneity: definition of enriched and depleted Caribbean endmembers*

As has been discussed above, both the Sr and Pb isotope systems have been affected to some extent by seawater alteration/metamorphism and crustal contamination. If we exclude samples affected by these processes from consideration, the CLIP basalts, including data from Gorgona, form positive correlations on Pb isotope diagrams and negative correlations on Nd versus Pb and possibly Sr isotope correlation diagrams (Figs. 3 and 5). The Nd isotope ratios, which are most resistant to alteration of the studied isotope ratios, correlate positively with Mg# in samples with $MgO > 8.0$ wt% (not shown) and form good inverse correlations with ratios of highly incompatible, immobile trace elements where the more incompatible element is in the numerator, such as Th/La, La/Ce, Ce/Sm and Nd/Sm (e.g. Fig. 6). The Gorgona tuffs and picrites, however, are off-set to lower ratios of more to less incompatible elements with larger differences in degree of incompatibility (e.g. Ce/Sm, Nd/Sm, Fig. 7a), which could reflect depletion of the source by previous melt extraction shortly before generation of these melts [34]. These correlations suggest that at least two components distinct in major element, trace element and isotopic composition contribute to the formation of the CLIP.

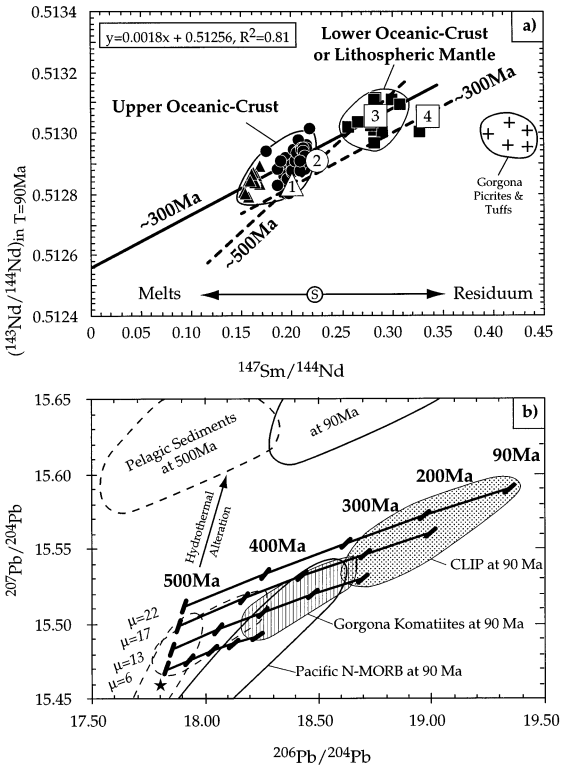

Fig. 7. The temporal constraints of the Sm–Nd and U–Pb isotope systematics are interpreted to reflect recycling of oceanic lithosphere through the deeper mantle back to the surface ≤500 Ma. (a) Transitional tholeiites (▲), tholeiites (●) and depleted komatiites (■) of the CLIP fall on a Sm–Nd reference isochron of ~300 Ma (solid line). Horizontal arrows denote element fractionation of Sm/Nd in the melt and the residual source during partial melting. These effects were modelled for a source (S) in the garnet and spinel stability field for batch melting and pooled fractional melting after [44]. Large open symbols with numbers correspond to modelled source compositions (1 = transitional tholeiites, 2 = tholeiites and 3, 4 = komatiites) and dashed lines to the corresponding source isochrons discussed in the text. (b) Evolution of U–Pb isotope systematics in the CLIP source. The μ values of the freshest CLIP tholeiites and transitional tholeiites range from 10 to 30. The Gorgona komatiites have considerably lower μ values of 5–6 and are similar to those estimated for DMM [26]. Fields with solid lines are corrected for 90 Ma of radioactive decay; those with dashed lines are corrected for 500 Ma. The fields for Pacific N-MORB are based on literature data (**EPSL Online Background Dataset**, see footnote 1). At 500 Ma $^{206}Pb/^{204}Pb$ in the CLIP sources spreads over a relatively narrow range (~17.8 to ~17.9) that overlaps with the estimated composition of Pacific N-MORB and DMM (**EPSL Online Background Dataset**, see footnote 1; see text for details). Higher $^{207}Pb/^{204}Pb$ isotope ratios and μ values in the CLIP source as expected for Pacific N-MORB could reflect hydrothermal alteration of the ocean crust at 500 Ma.
←

CLIP lavas with enriched or depleted geochemical characteristics only occur at a few localities. Lavas with enriched incompatible trace element and isotopic compositions include samples from DSDP Site 151, the Dumisseau Formation on Haiti and tholeiitic basalts from Gorgona Island (**EPSL Online Background Dataset**, see footnote 1). Volcanic samples from Quepos, which are believed to have formed above the plume stem at 60–65 Ma [11,35], also have enriched trace element and isotopic compositions. Lavas depleted in incompatible elements and isotopic composition include komatiites, picrites and D-basalts from Gorgona (90 Ma) and lavas from DSDP Site 152 (~75 Ma), the Siete Cabezas Formation in the Dominican Republic (69 Ma) and the Osa aseismic ridge (63 Ma). The small island of Gorgona is exceptional within the CLIP, because depleted and enriched lavas were erupted contemporaneously at ~90 Ma [9,36], showing that chemical variations do not only reflect temporal evolution within the plume head.

In conclusion, the enriched Caribbean endmember is observed primarily in transitional tholeiitic rocks and is characterized by (1) low Mg# (53–61), (2) enrichment in highly and moderately incompatible elements relative to the less incompatible elements, and (3) radiogenic Pb ($(^{206}Pb/^{204}Pb)_{in} \geq 19.2$; $(^{208}Pb/^{204}Pb)_{in} \geq 38.9$) and Sr ($(^{87}Sr/^{86}Sr)_{in} \geq 0.7032$, if we accept that the Sr isotope ratios of the least radiogenic samples reflect the source composition, but unradiogenic Nd ($(^{143}Nd/^{144}Nd)_{in} \leq 0.5128$) isotope compositions. The depleted Caribbean endmember, as represented by the Gorgona komatiites and picrites, has very high Mg# (>75), is extremely depleted in highly and moderately incompatible elements and contains unradiogenic Pb ($(^{206}Pb/^{204}Pb)_{in} \leq 18.4$; $(^{208}Pb/^{204}Pb)_{in} \leq 37.9$) and Sr ($(^{87}Sr/^{86}Sr)_{in} \leq 0.7027$, lowest value in the Gorgona komatiites), but radiogenic Nd ($(^{143}Nd/^{144}Nd)_{in} \geq 0.5131$).

4.3. Origin of enriched and depleted Caribbean endmembers from recycled oceanic lithosphere

As noted in Section 4.2, at least two components are required to explain differences in major element, trace element and isotopic composition. A decrease in $^{143}Nd/^{144}Nd$ and increase in La/Ce and Th/La with decreasing Mg# could possibly reflect assimilation of oceanic sediments during fractional crystallization (AFC) from komatiite to transitional tholeiite. Sediment assimilation, however, should also cause significant depletion in Nb and Ta relative to other highly incompatible elements such as Th, K and La and enrichment in Pb relative to Ce and Nd [17]. As is illustrated in Fig. 2a,b, however, the opposite is observed! Nb and Ta in the transitional tholeiites show the greatest enrichment relative to all other incompatible elements and Pb is depleted compared to most other incompatible elements. These geochemical features are characteristic of ocean island basalts instead of sediments.

Alternatively both the enriched and depleted endmembers could be generated by melting of at least two distinct mantle sources at 90 Ma. The geochemistry of the enriched Caribbean endmember is consistent with derivation from recycled oceanic crust. Although the relatively low Mg# of this endmember does not have to represent a primary source characteristic, mantle pyroxenite, which may represent recycled oceanic crust [20], extends to similarly low Mg# [37]. In addition, the enriched Caribbean endmember has incompatible trace element characteristics similar to OIB, showing affinities in particular to the HIMU endmember in OIB as is illustrated for example on diagrams of La/Nb versus Zr/Nb (Fig. 2c) and Ba/Nb and by the high μ ratios up to 30 in fresh samples. The $^{143}Nd/^{144}Nd$ and the lowest $^{87}Sr/^{86}Sr$ ratios in the transitional tholeiites are also similar to those in HIMU-type basalts. The HIMU endmember in OIB is commonly believed to represent ancient (ca. 2 Ga) recycled oceanic crust (e.g. [38,39]). Although the Pb isotopic compositions of the enriched Caribbean lavas are less radiogenic than endmember HIMU, they are higher than MORB and EM I-type OIB and indicate elevated time-integrated μ in the source. Two possible explanations for the less radiogenic Pb in the Caribbean enriched endmember are (1) mixing of HIMU with another component with unradiogenic Pb (e.g. depleted mantle), or (2) derivation from young (≤ 1 Ga) recycled ocean crust. It has been shown that young recycled ocean crust can have positive $\Delta 7/4$Pb (i.e. $^{207}Pb/^{204}Pb$ above the NHRL) as observed for the CLIP lavas (Fig. 3b) if hydrothermal alteration has added crustal Pb in addition to increasing the U/Pb ratio [20,27]. In fact, Jurassic (~ 170 Ma) ocean crust samples from beneath the Canary Islands have compositions that almost completely overlap the Pb isotopic compositions of the Caribbean tholeiites [20]. In conclusion, the major element, trace element and isotopic compositions of the enriched endmember are consistent with derivation from recycled oceanic crust.

The $^{3}He/^{4}He$ ratios (~ 12 R_A) in fresh olivines from the Quepos picrites are higher than have been found in MORB or endmember HIMU thus far (≤ 9 R/R_A) (e.g. [40]) but fall within the range found at the Galápagos Islands, which have similar Sr–Nd–Pb isotopic compositions to CLIP and have also been interpreted to be derived from recycled crustal material [29]. Whereas endmember HIMU with low $^{3}He/^{4}He$ ratios (6.8 ± 0.9 R/R_A) may have only been recycled to the upper/lower mantle boundary [40], the elevated $^{3}He/^{4}He$ ratios of the Quepos picrites and the high γOs in some of the enriched picrites and tholeiites from Curaçao [36] suggest recycling of the enriched Caribbean endmember into the lower mantle, possibly to the core–mantle boundary.

The depleted Sr–Nd–Pb isotope characteristics of the depleted Caribbean endmember indicate derivation from a mantle source with a long-term history of depletion, such as the MORB source. The extreme major and trace element depletion of the Gorgona komatiites and picrites, in particular when compared to MORB (Fig. 2a,b), would require additional source depletion some time in the relatively recent past (200–300 Ma) or the Nd isotope ratios would be considerably higher than those measured, as a result of the very high Sm/Nd ratios in these rocks [34]. One possibility is that these rocks were derived from a residual MORB source, such as oceanic litho-

spheric mantle formed at a mid-ocean ridge from the residuum remaining after melt extraction to form the oceanic crust (e.g. [34,41]). Alternatively the komatiites might be derived from the melting of recycled lower oceanic crust, consisting of gabbroic cumulates interlayered with mafic to ultramafic cumulates. Since the lower crust is not affected by extensive hydrothermal alteration at the mid-ocean ridge, it will be extremely depleted in all incompatible elements, have very low Rb/Sr, U/Pb and Th/Pb but very high Sm/Nd, and will have an isotopic composition similar to MORB if the recycling time is relatively short (≤ 500 Ma).

Melting of mafic lower crust and lithospheric mantle requires mantle temperatures well in excess of those expected in the Cretaceous upper mantle. The high MgO content and spinifex textures of the Gorgona komatiites, however, indicate eruption temperatures in the order of 1360–1400°C [34] and serve as minimum melting temperatures. Temperatures in excess of 1400°C are sufficient to melt even a refractory source. Recycling of the oceanic lithosphere through the lower mantle serves as a possible mechanism for heating oceanic lithosphere to such temperatures. Support for lower mantle recycling of the depleted Caribbean endmember comes from high γOs (up to +12.4) in the komatiites and picrites from Gorgona [36,42].

In conclusion, both the enriched and depleted endmembers in the Caribbean starting plume head could represent oceanic lithosphere recycled through the lower mantle. However, it cannot be ruled out that depleted upper mantle was involved in the formation of the younger depleted lavas at DSDP Site 152 ($\sim$75 Ma), the Siete Cabezas Formation in the Dominican Republic (69 Ma) and the Osa igneous complex in Costa Rica (63 Ma), since there are no Os or He isotope data available for these samples. Depleted upper mantle may have upwelled and melted beneath DSDP Site 152 and the Dominican Republic between 69 and 75 Ma as a result of lithospheric extension caused by gravitational collapse of the over-thickened plateau crust [9]. The depleted material found at Osa may reflect melting of upper mantle entrained into the plume or may reflect plume–ridge interaction, as has been proposed to explain the chemical zonation observed at the Galápagos Islands (e.g. [31,32]).

4.4. Constraints on recycling times for oceanic lithosphere via plume heads: implications for upper mantle composition

If the Caribbean enriched and depleted endmembers reflect different parts of recycled oceanic lithosphere, then they could have been derived from a common reservoir, the depleted MORB source mantle (DMM), at a similar time in the past. In this respect, evaluation of isotope systems on isochron diagrams can be used to place temporal constraints. The immobile nature of Sm and Nd makes this system particularly resistant to seafloor alteration/metamorphism and the subduction process. Initial Nd isotope data correlate positively with measured $^{147}Sm/^{144}Nd$ for volcanic rocks from the CLIP, excluding the Gorgona tuffs and picrites. The linear regression (solid line in Fig. 7a) fitted to the data ($R^2 = 0.81$) yields an age of $\sim$300 Ma and an initial $^{143}Nd/^{144}Nd$ of 0.51256. If the CLIP basalts are formed by relatively large degrees of partial melting ($\geq 15\%$ batch melting or fractional melting), then their $^{147}Sm/^{144}Nd$ ratios will be similar to those in the source at 90 Ma and the correlation on the Sm–Nd isochron diagram could reflect an average age of $\sim$300 Ma for the separation from a common source.

At lower degrees of melting, the $^{147}Sm/^{144}Nd$ ratios of the CLIP basalts will be lower than in the source at 90 Ma. If the transitional tholeiites and tholeiites formed at lower degrees of melting than the komatiites and the transitional tholeiites, which have steep chondrite-normalized HREE patterns and formed with garnet in their residuum [11], then the source is likely to form a steeper array on the Sm–Nd isochron diagram than the melts. Assuming that the tholeiites formed by 10–15% batch or fractional melting in the spinel stability field, which serves as a lower limit for the generation of MORB tholeiites (e.g. [43]), and the transitional tholeiites by 6–8% batch melting in the garnet stability field, then the resulting three-point source isochron (dashed isochron going through sources of transitional tho-

leiites (triangle with 1), tholeiites (circle with 2) and komatiites (square with 3) will have a slope corresponding to an age of ~500 Ma. We believe that significantly lower degrees of melting than assumed above for the tholeiites and transitional tholeiites are unlikely.

Accepting that melting to form the CLIP tholeiites is not significantly below 10%, then the only way that a common source for CLIP could be older than ~500 Ma is if the komatiite source has lower $^{147}Sm/^{144}Nd$ ratios than the komatiitic melts. This would be possible if small-degree fractional melts were removed from the komatiite source shortly before generation of the komatiitic melts, such that the komatiites represent melts of residual source material [34]. The first melts of the original komatiitic source should then have lower $^{147}Sm/^{144}Nd$ ratios but similar $^{143}Nd/^{144}Nd$ ratios to the komatiites. Melts with such a composition, however, have not been reported from Gorgona. On the contrary, picrites and tuffs on Gorgona have similar $^{143}Nd/^{144}Nd$ ratios to the komatiites but higher $^{147}Sm/^{144}Nd$ ratios and thus are most likely to have been derived from the residue left after melt extraction to form the komatiites [34]. The common source of the komatiites and picrites/tuffs would then lie between the data arrays of these melts (square with 4 in Fig. 7a) and is in the range of oceanic lithospheric mantle left after formation of the oceanic crust [44]. This scenario, coupled with the melting process discussed above, aligns the source isochron more or less parallel to the melt isochron and gives an age of ≤300 Ma (300 Ma dashed isochron in Fig. 7a). Accepting that the CLIP basalts were derived from oceanic lithosphere which formed at a similar time, then ~500 Ma serves as a reasonable upper age limit for this lithosphere.

The U–Pb isotope systematics are also consistent with derivation of the CLIP source from DMM within a relatively short time frame (< 500 Ma). As noted previously, systematic variations exist between both Pb isotopic composition and μ and lava chemistry. The Gorgona komatiites have the least radiogenic Pb isotopic composition (Figs. 5 and 7b) and the lowest μ (5–6) whereas the tholeiites and transitional tholeiites have more radiogenic Pb and higher μ (10–30, when only the freshest samples are considered). In Fig. 7b, we present a model that shows that the Pb isotopic composition of all CLIP lavas could be generated from DMM within the last 500 Ma. The initial composition of the DMM source (denoted by a star in Fig. 7b) was estimated assuming that the average present composition of Pacific N-MORB (with $^{206}Pb/^{204}Pb = 18.4$ and $^{207}Pb/^{204}Pb = 15.49$) has evolved with a μ of 7 [45] for the last 500 Ma. The model further assumes that the upper oceanic crust was hydrothermally altered shortly after formation which could have caused an increase in (a) μ (6–22) through Pb leaching and/or U gain and (b) $^{207}Pb/^{204}Pb$ (15.46–15.51) through exchange with crustal Pb from oceanic sediments or seawater [20,24,26]. Radioactive decay of U over ~400 Ma is then capable of generating the observed range in Pb isotopic composition of CLIP at the time of formation (90 Ma ago).

In summary, the geochemistry of the CLIP basalts is interpreted to record a complex history of recycling of oceanic lithosphere and alteration/metamorphism after eruption of the lavas on the seafloor. The recycling process includes generation of oceanic lithosphere at a mid-ocean ridge, alteration/metamorphism of the upper crust on the seafloor, subduction of the lithosphere into the lower mantle, residence and contamination (of at least He and Os) in the lower mantle, rise to the surface in the Galápagos starting plume head and finally melting at the base of Jurassic lithosphere. Considering the effects of melting and hydrothermal alteration on the Sm–Nd and U–Pb isotope systems respectively, the average recycled oceanic lithosphere could have formed within 300–500 Ma before the Caribbean flood basalt event. This would further imply that starting plume heads can facilitate the recycling of large volumes (possibly in the order of 10^6 km^3 or greater) of oceanic lithosphere within a few hundred million years. Studies on the Pb isotopic composition of global MORB [27] and on Jurassic oceanic crust beneath the Canary Islands [20] have shown that even the Pb isotopic composition of the HIMU endmembers could develop within 200–300 Ma, suggesting that recycling times for oceanic crust can be far shorter than the com-

monly suggested ~2 Ga. Injection of large volumes of relatively young oceanic lithosphere into the upper mantle by mid-Cretaceous plume heads from the lower mantle would be expected to have affected the composition of the present upper mantle MORB source. Interestingly, it has been suggested that the C component, an endmember in the global MORB Pb isotope data set, reflects the presence of a relatively young (≥300 Ma) recycled ocean crust component in the MORB source [27]. In this respect, mid-Cretaceous starting plume heads may represent a possible mechanism for large-scale mass transfer that have replenished the upper mantle with young oceanic lithosphere recycled through the lower mantle.

5. Conclusions

This study integrates trace element and Sr–Nd–Pb–He isotope data of widely distributed lavas of the Caribbean oceanic plateau and its subsequent hotspot track into a model for the origin and evolution of starting plume heads. We show that:

1. Seawater alteration variably affects the trace element and isotopic composition in whole rock samples of submarine lavas. The Sm–Nd isotope system is least affected by seawater alteration. Rb and Sr show the highest degree of element mobility. Although the majority of samples have undisturbed U–Th–Pb systematics, alteration, in particular hydrothermal alteration, has affected the concentrations of U and Pb and the $^{238}U/^{204}Pb$, $^{232}Th/^{204}Pb$, Nd/Pb, Ce/Pb and Nb/U ratios of some samples. Since the initial Pb isotope ratios between the altered and unaltered lavas are similar, hydrothermal alteration appears to have been primarily active within several million years of the flood basalt event. Considering the large volumes of lavas erupted over relatively short geological time scales during flood basalt events, the resulting hydrothermal systems are expected to have a major effect on the chemistry of the world's oceans.
2. The similarity in chemical composition of the flood basalts and the subsequent hotspot track (to about 60 Ma) with the present lavas forming the Galápagos Islands supports generation of the CLIP from the Galápagos starting plume head.
3. Correlations between major elements, trace elements and isotope ratios indicate that at least two components were involved in the generation of the CLIP. Both components can be derived from recycled oceanic lithosphere with the enriched component representing recycled, altered upper oceanic crust and the depleted component unaltered lower oceanic crust or oceanic lithospheric mantle. High ^{3}He isotope signatures of the enriched component indicate residence within the lower mantle, possibly at the core–mantle boundary.
4. The Sm–Nd and U–Pb isotope systematics indicate that the source components could have separated from a common DMM-like mantle some time within the 300–500 Ma before the formation of the CLIP and interpreted to reflect the recycling age of this oceanic lithosphere. We propose that multiple mid-Cretaceous starting plume heads could have caused large volume contamination of the upper mantle with young recycled oceanic lithosphere, which is also evident in the chemistry of recent MORB [27].

Acknowledgements

We thank G. Alvarado (ICE, Costa Rica), R. Werner, H.-U. Schmincke (GEOMAR) and J. Tarney (University of Leicester) for valuable help during field work and for providing logistical and financial support. T.W. Donnelly (SUNY, Binghamton, NY, USA) kindly donated samples from DSDP Leg 15. D. Garbe-Schönberg, T. Arpe and H. Blaschek (Geological Institute, University of Kiel) are thanked for their help with ICP–MS analyses and K. Wolff for their help with the XRF analyses. F.H. appreciates support from the German Academic Exchange Service (DAAD) through an overseas scholarship to carry out TIMS analyses partly at UCSB. This publication is part of the Ph.D thesis of F.H. and the TICOSECT project, both funded by the Deutsche

Forschungsgemeinschaft (DFG). Helpful and critical reviews by E. Kogiso, F. Frey and N. Arndt are gratefully acknowledged. *[CL]*

Appendix A. Analytical methods

Samples studied for Sr–Nd–Pb isotopic composition generally have LOI <2.0 wt% except for DSDP Leg 15 samples with LOI of up to 2.6 wt%. Major elements (SiO_2, Al_2O_3, MgO, Fe_2O_3, CaO, Na_2O, K_2O, TiO_2, MnO and P_2O_5) and some trace elements (Cr, Ni, Zr, Sr) were determined on fused beads using a Philips X'Unique PW1480 X-ray fluorescence spectrometer (XRF) equipped with a Rh tube at GEOMAR. Additional trace elements (Rb, Ba, Y, Nb, Ta, Hf, U, Th, Pb and all REE) were determined by ICP–MS on a VG Plasmaquad PQ1 ICP–MS at the Geological Institute of the University of Kiel after the methods of Garbe-Schönberg [46]. The accuracy of reference material BIR-1 and BHVO-1, measured along with the samples, is within $\pm 10\%$ of the suggested working values [47,48], but generally better than 5% for REE. Sr, Nd, Pb isotope ratios and U–Th–Pb concentrations by isotope dilution analyses were carried out on a Finnigan MAT 262-RPQ2+ at GEOMAR Research Center and on a Finnigan MAT 261 thermal ionization mass spectrometer at the Department of Geological Sciences at the University of California in Santa Barbara (UCSB). Replicate analyses of Sr–Nd–Pb isotopes on the same samples analyzed at GEOMAR and UCSB were within the analytical uncertainties and no systematic interlaboratory bias was apparent. Sr was measured in static mode and $^{87}Sr/^{86}Sr$ normalized within-run to $^{86}Sr/^{88}Sr = 0.1194$. NBS987 gave a $^{87}Sr/^{86}Sr$ ratio of 0.710247 ± 6 ($n = 15$) at GEOMAR. Samples (151-2, 152-1, 153-1, SDB16) measured at UCSB were normalized to NBS987. A subset of samples were leached for 3 h in a mix of 50% 6 N HCl and 50% 8 N HNO_3 for Sr isotope analyses. The initial $^{87}Sr/^{86}Sr$ of the leached samples are displayed in italics and calculated taking Rb, Sr concentrations of the unleached sample. Note that the age corrections of the Rb–Sr system are relatively minor in these rocks. The $^{143}Nd/^{144}Nd$ ratio was normalized within-run to $^{146}Nd/^{144}Nd = 0.7219$ and measured in static mode at GEOMAR where the Nd standard La Jolla yielded an average ratio of $^{143}Nd/^{144}Nd = 0.511847 \pm 4$ ($n = 12$); at UCSB the AMES standard gave a $^{143}Nd/^{144}Nd$ ratio of 0.511893 ± 10 ($n = 25$) compared to the long-term ratio of 0.511889 ± 9 in this lab. Analyses of NBS981 ($n = 20$) at GEOMAR gave $^{206}Pb/^{204}Pb = 16.892 \pm 5$, $^{207}Pb/^{204}Pb = 15.431 \pm 6$ and $^{208}Pb/^{204}Pb = 36.509 \pm 19$. At UCSB NBS981 yielded $^{206}Pb/^{204}Pb = 16.896 \pm 6$, $^{207}Pb/^{204}Pb = 15.433 \pm 8$ and $^{208}Pb/^{204}Pb = 36.522 \pm 24$, ($n = 51$). All Pb isotope analyses were corrected to NBS981 [49] for fractionation. Total chemistry blanks in both labs were <0.3 ng for Pb, <0.2 ng for Sr and <0.06 ng for Nd, Th, U and thus negligible. Replicate analyses of 16 samples gave an external reproducibility better than 0.03% per amu for Pb and <0.000015 for $^{143}Nd/^{144}Nd$ and $^{87}Sr/^{86}Sr$. The external reproducibility of U–Th–Pb concentration determinations by isotope dilution is better than 1% based on 16 samples while that for Sm–Nd is $<2\%$ and that for Rb–Sr is $<4\%$. All errors and standard deviations in this manuscript are given at the 2σ confidence level. Helium isotope ratios of olivine separates were analyzed in the Pacific Marine Environment Laboratory at NOAA using the methods described by Graham et al. [33].

References

[1] M.A. Richards, R.A. Duncan, V.E. Courtillot, Flood basalts and hot spot tracks: Plume heads and tails, Science 246 (1989) 103–107.
[2] R.W. Griffiths, I.H. Campbell, Stirring and structure in mantle plumes, Earth Planet. Sci. Lett. 99 (1990) 66–78.
[3] C.G. Farnetani, M.A. Richards, Numerical investigations of the mantle plume initiation model, J. Geophys. Res. 99 (1994) 13813–13833.
[4] D. Bercovici, A. Kelly, The non-linear initiation of diapirs and plume heads, Phys. Earth Planet. Interact. 101 (1997) 119–130.
[5] R.L. Larson, Latest pulse of Earth: Evidence for a mid-Cretaceous superplume, Geology 19 (1991) 547–550.
[6] R.A. Duncan, R.B. Hargraves, Caribbean region in the mantle reference frame, in: W. Bonini, R.B. Hargraves, R. Shagam (Eds.), The Caribbean-South American Plate Boundary and Regional Tectonics, 162, Geological Society of America Memoir, Boulder, CO, 1984, pp. 89–121.

[7] A.C. Kerr, J. Tarney, G.F. Marriner, A. Nivia, A.D. Saunders, The Caribbean-Colombian Igneous Province: The internal anatomy of an oceanic plateau, in: J.J. Mahoney, M.F. Coffin (Eds.), Large Igneous Provinces, Geophysical Monograph 100, AGU, Washington, DC, 1997, pp. 123–144.
[8] T.W. Donelly, W. Melson, R. Kay, J.J.W. Rogers, Basalts and dolerites of late Cretaceous age from the Central Caribbean, Init. Rep. DSDP 15 (1973) 989–1012.
[9] C.W. Sinton, R.A. Duncan, M. Storey, J. Lewis, J.J. Estrada, An oceanic flood basalt province within the Caribbean plate, Earth Planet. Sci. Lett. 155 (1998) 221–235.
[10] A. Maufrett, S. Leroy, Seismic stratigraphy and structure of the Caribbean igneous province, Tectonophysics 293 (1997) 61–104.
[11] F. Hauff, K. Hoernle, H.-U. Schmincke, R. Werner, A mid Cretaceous origin for the Galápagos Hotspot: Volcanological, petrological, and geochemical evidence from Costa Rican oceanic crustal segments, Geol. Rundsch. 86 (1997) 141–155.
[12] J.L. Pindell, S.F. Barrett, Geological evolution of the Caribbean region; a plate tectonic perspective, in: G. Dengo, J.E. Case (Eds.), The Caribbean Region, The Geology of North America H, Geological Society of America, Boulder, CO, 1990, pp. 405–432.
[13] M. Meschede, W. Frisch, A plate tectonic model for the Mesozoic and Early Cenozoic history of the Caribbean plate, Tectonophysics 296 (1998) 269–291.
[14] H. Montgomery, E.A. Pessagno, J.L. Pindell, A 195 Ma terrane in 165 Ma sea Pacific origin of the Caribbean plate, GSA Today 4 (1994) 3–7.
[15] W. Frisch, M. Meschede, M. Sick, Origin of the Central American ophiolites: Evidence from paleomagnetic results, Geol. Soc. Am. Bull. 104 (1992) 1301–1314.
[16] K. Hoernle, U. Schweikert, R. Werner, P. v.d. Bogaard, The Caribbean flood basalt event and the missing link the Galápagos hotspot: preliminary results from Panama, Terra Nostra 5 (1998) 69.
[17] A.W. Hofmann, Chemical differentiation of the Earth: the relationship between mantle, continental and oceanic crust, Earth Planet. Sci. Lett. 90 (1988) 297–314.
[18] F. Hauff, Age and Geochemical Constraints on the Origin of Oceanic Basement Complexes in Costa Rica and the Caribbean Large Igneous Province, Ph.D. Thesis, University of Kiel, 1998.
[19] S.-s. Sun, W.F. McDonough, Chemical and isotopic systematics of oceanic basalts: implications for mantle composition and processes, in: A.D. Saunders, M.J. Norry (Eds.), Magmatism in the Ocean Basins, Geological Society London Special Publication 42, Blackwell, London, 1989, pp. 313–345.
[20] K. Hoernle, Geochemistry of Jurassic oceanic crust beneath Gran Canaria (Canary Islands): Implications for crustal recycling and assimilation, J. Petrol. 39 (1998) 859–880.
[21] J.J. Mahoney, K.J. Spencer, Isotopic evidence for the origin of the Manihiki and Ontong Java oceanic plateaus, Earth Planet. Sci. Lett. 104 (1991) 196–210.
[22] A.C. Kerr, J. Tarney, G.F. Marriner, G.T. Klaver, A.D. Saunders, M.F. Thirlwall, The geochemistry and petrogenesis of the late-Cretaceous picrites and basalts of Curaçao, Netherlands Antilles: a remnant of an oceanic plateau, Contr. Mineral. Petrol. 124 (1996) 29–43.
[23] P.E. Janney, P.R. Castillo, Geochemistry of Mesozoic Pacific mid-ocean ridge basalt: constraints on melt generation and the evolution of the Pacific upper mantle, J. Geophys. Res. 102 (1997) 5207–5229.
[24] H. Staudigel, G.R. Davies, S.R. Hart, K.M. Marchant, B.M. Smith, Large scale isotopic Sr, Nd and O isotopic anatomy of altered oceanic crust: DSDP/ODP sites 417/418, Earth Planet. Sci. Lett. 130 (1995) 169–185.
[25] M. Rehkämper, A.W. Hofmann, Recycled ocean crust and sediment in the Indian Ocean MORB, Earth Planet. Sci. Lett. 147 (1997) 93–106.
[26] W.M. White, $^{238}U/^{204}Pb$ in MORB and open system evolution of the depleted mantle, Earth Planet. Sci. Lett. 115 (1993) 211–226.
[27] B.B. Hanan, D.W. Graham, Lead and helium isotope evidence from oceanic basalts for a common deep source of mantle plumes, Science 272 (1996) 991–995.
[28] S.R. Hart, A large-scale isotope anomaly in the Southern Hemisphere mantle, Nature 309 (1984) 753–757.
[29] D.W. Graham, D.M. Christie, K.S. Harpp, J.E. Lupton, Mantle plume helium in submarine basalts from the Galapagos Platform, Science 262 (1993) 2023–2026.
[30] R. Werner, K. Hoernle, P. v.d. Bogaard, C. Ranero, R. Huenev, A drowned 14 Ma old Galápagos Archipelago off the coast of Costa Rica: Implications for evolutionary and tectonic models, Geology 27 (1999) 499–502.
[31] J.-G. Schilling, R.H. Kingsley, J.D. Devine, Galapagos hot spot-spreading center system 1. Spatial petrological and geochemical variations (83°W–101°W), J. Geophys. Res. 87 (1982) 5593–5610.
[32] W.M. White, A.R. McBirney, R.A. Duncan, Petrology and geochemistry of the Galápagos Islands: Portrait of a pathological mantle plume, J. Geophys. Res. 98 (1993) 19533–19563.
[33] D.W. Graham, L.M. Larsen, B.B. Hanan, M. Storey, A.K. Pedersen, K.E. Lupton, Helium isotope composition of the Early Iceland Mantle Plume inferred from Tertiary picrites of West Greenland, Earth Planet. Sci. Lett. 160 (1998) 241–255.
[34] N.T. Arndt, A.C. Kerr, J. Tarney, Dynamic melting in plume heads: the formation of Gorgona komatiites and basalts, Earth Planet. Sci. Lett. 146 (1997) 289–301.
[35] C.W. Sinton, R.A. Duncan, P. Denyer, Nicoya Peninsula, Costa Rica: a single suite of Caribbean oceanic plateau magmas, J. Geophys. Res. 102 (1997) 15507–15520.
[36] R.J. Walker, M. Storey, A.C. Kerr, J. Tarney, N.T. Arndt, Implications of 187 Os heterogeneities in a mantle plume: Evidence from Gorgona Island and Curaçao, Geochim. Cosmochim. Acta 63 (1999) 713–728.
[37] M.M. Hirschmann, E.M. Stolper, A possible role for gar-

net pyroxenite in the origin of the 'garnet signature' in MORB, Contr. Mineral. Petrol. 124 (1996) 185–208.
[38] C.G. Chase, Oceanic island Pb: two stage histories and mantle evolution, Earth Planet. Sci. Lett. 52 (1981) 277–284.
[39] A.W. Hofmann, W.M. White, Mantle plumes from acient oceanic crust, Earth Planet. Sci. Lett. 57 (1982) 421–436.
[40] T. Hanyu, I. Kaneoka, The uniform and low $^{3}He/^{4}He$ ratios of HIMU basalts as evidence for their origin as recycled materials, Nature 390 (1997) 273–276.
[41] A.C. Kerr, A.D. Saunders, J. Tarney, N.H. Berry, V.L. Hards, Depleted mantle-plume geochemical signatures: No paradox for plume theories, Geology 23 (1995) 843–846.
[42] R.J. Walker, L.M. Echeverría, S.B. Shirey, M.F. Horan, Re-Os isotopic constraints on the origin of volcanic rocks, Gorgona island, Colombia: Os isotopic evidence for acient heterogeneties in the mantle, Contr. Mineral. Petrol. 107 (1991) 150–162.
[43] E.M. Klein, C.H. Langmuir, Global correlations of ocean ridge basalt chemistry with axial depth and crustal thickness, J. Geophys. Res. 92 (1987) 8089–8115.
[44] K.T. Johnson, H.J.B. Dick, N. Shimizu, Melting in the oceanic upper mantle: An ion microprobe study of diopsides in abyssal peridotites, J. Geophys. Res. 95 (1990) 2661–2678.
[45] M.F. Thirlwall, Pb isotopic and elemental evidence for OIB derivation from young HIMU mantle, Chem. Geol. 139 (1997) 51–74.
[46] C.-D. Garbe-Schönberg, Simultaneous determination of thirty-seven trace elements in twenty-eight international rock standarts by ICP-MS, Geostandard Newslett. 17 (1993) 81–97.
[47] K. Govindaraju, Compilation of working values and sample descriptions for 383 geostandards, Geostandard Newslett. 18 (1994).
[48] K.-P. Jochum, H.M. Seufert, M.F. Thirlwall, Multi-element analyses of 15 international standard rocks by isotope dilution spark source mass spectrometry, Geostandard Newslett. 14 (1990) 469–473.
[49] W. Todt, R.A. Cliff, A. Hanser, A.W. Hofmann, Evaluation of a ^{202}Pb-^{205}Pb double spike for high precision lead isotope analyses, in: A. Basu, S. Hart (Eds.), Earth Processes: Reading the Isotopic Code, Geophysical Monograph 95, AGU, Washington, DC, 1996, pp. 429–437.
[50] T. Plank, C.H. Langmuir, The chemical composition of subducting sediment and its consequences for the crust and mantle, Chem. Geol. 145 (1998) 325–394.
[51] B.L. Weaver, The origin of ocean island basalt end-member compositions: trace element and isotopic constraints, Earth Planet. Sci. Lett. 104 (1991) 381–397.
[52] K. Hoernle, H.-U. Schmincke, The petrology of the tholeiites through melilite nephelinites on Gran Canaria, Canary Islands: crystal fractionation, accumulation, and depths of melting, J. Petrol. 34 (1993) 573–597.
[53] G.R. Tilton, Evolution of depleted mantle: the lead perspective, Geochim. Cosmochim. Acta 47 (1983) 1191–1197.

Background Information for EPSL-Online

General Geology of the Studied CLIP Areas

DSDP Leg 15

Conformably overlying Conician strata and $^{40}Ar/^{39}Ar$ age data indicate that the basalts and dolerites at Site 146, 150, 151 and 153 formed shortly before 88 Ma and that basalts at Site 152 formed in the Late Campanian (~75 Ma [1, 2]). Site 152 is located between the Hess escarpment and the Beata ridge above oceanic crust that is thinner than found in the Colombian and Venezuelan basins. The structural setting has been interpreted to result from the gravitational collapse and extension of over-thickened plateau crust [2]. The petrography of the Leg 15 basalts indicates various degrees of alteration as well as sediment assimilation, for example micaceous amygdale fillings, alteration of glass to saponite and marble xenoliths at Site 152 [1]. Previous studies have noted that the Leg 15 basalts range in composition from incompatible element enriched (Site 151) to slightly depleted (Site 146, 150, 153) to strongly depleted signatures at Site 152 (e.g. [1, 3].

Curaçao

The Curaçao lava sequence is 5km thick, consisting of picritic and tholeiitic pillow basalts with minor occurrences of hyaloclastites and dikes ([4]and references therein). Two basalts, from the lower and upper part of the volcanic sequence, yield $^{40}Ar/^{39}Ar$ plateau ages of ~90 Ma [2]. The lava flows become more differentiated up-section and geochemical modelling has shown that the picrites and tholeiites can be related through fractional crystallisation of olivine, clinopyroxene and plagioclase. The slightly less radiogenic Nd isotopic character of the picrites than the tholeiites has been related to either small scale source heterogeneity or (less likely) to assimilation of a crustal component by the picrites [4].

Colombia

Gravity anomalies show that the Romeral fault is a major terrane boundary, separating continental crust in the east from several north-south trending oceanic terranes in the west [5]. Basaltic rocks of the Western Cordillera have been dated by $^{40}Ar/^{39}Ar$ at 91.7±2.7 Ma in agreement with intercalated Touronian/Conician (91-87.5Ma) sediments and at 76.5±1.6 Ma, while Serranía de Baudó volcanic rocks range from 72-78 Ma [2, 5]. Geochemical modelling and Sr-Nd isotope data are interpreted to reflect derivation of both lava series through polybaric melting of a heterogeneous plume [5]. The small island of Gorgona (2.5x8km) off the coast of Colombia ranges in age from 86-88 Ma [2, 6, 7] and contains the only well-documented Phanerozoic examples of komatiites, which are associated with tholeiitic basalts, gabbros, picrites and ultramafic tuffs [8]. Previous workers have subdivided the tholeiitic rocks on Gorgona into **d**epleted, "**k**omatiite-like" (D-, K-), **t**ransitional (T-) and **e**nriched (E-) basalts [6, 8, 9]. Despite the small size of Gorgona, its volcanic rocks show a relatively large range in major element, trace element and Sr-Nd-Pb-Os isotope composition [6, 7, 10-12], as discussed in more detail in the paper.

Costa Rica (92-75Ma) and (65-60Ma)

The Nicoya, Herradura, Golfito and Burica complexes along the Pacific coast of Costa Rica mark the westernmost exposures of the CLIP. These complexes are composed of aphyric pillow lavas, massive basalts, gabbros, plagiogranites and radiolarian chert. The volcanic facies of the extrusive rocks and high sulfur contents of fresh tholeiitic glasses indicate eruption in a deep marine environment [13]. Combined geochemical, petrological and $^{40}Ar/^{39}Ar$ age dating studies together with biostratigraphic evidence indicate that the vast majority igneous rocks formed between 92-75 Ma from a source compatible with the Galápagos hotspot [13, 14 and Hauff et al. manuscript in prep.]. The occurence of Jurassic and lower Cretaceous radiolarites on the Nicoya peninsula [15] are interpreted as remnants of the preexisting oceanic crust onto which the CLIP was emplaced. In contrast to other CLIP complexes, which seem to have formed at distinct pulses at ~90 Ma and ~75 Ma [2] continuous magmatism from 92 Ma through 75 Ma in the Costa Rican complexes may reflect the eastward migration of the western plateau margin over the plume stem.

The Quepos and Osa igneous complexes accreted to the Pacific margin of Costa Rica, formed between 65-60 Ma [Hauff et al. manuscript in prep.]. The volcanic stratigraphy of Quepos provides evidence for the emergence of a submarine volcanic edifice above sea level and the formation of an ocean island volcano. The volcanology, petrology and sedimentology of affiliated sediments suggests that the Osa igneous complex once formed part of an aseismic ridge similar to the Cocos Ridge presently being subducted beneath the Osa Peninsula. The Quepos and Osa igneous complexes are interpreted to be part of the subsequent hotspot track after the oceanic plateau migrated to the east. [13 Hauff et al. manuscript in prep.]. Eastward dipping subduction along the western margin of the CLIP (Centarl America) initiated at ~75 Ma and may result from differences in bouancy forces between normal oceanic and relatively young and hot plateau crust. Accretion of the Quepos and Osa complexes at ca. 45 Ma appears to have caused large-scale deformation throughout Central America [Hauff et al. manuscript in prep.] similar to the indention of the Cocos Ridge 5 Ma ago [16].

References

1. T.W. Donelly, W. Melson, R. Kay and J.J.W. Rogers, Basalts and dolerites of late Cretaceous age from the Central Caribbean, Init. Rep. DSDP 15, 989-1012, 1973.

2. C.W. Sinton, R.A. Duncan, M. Storey, J. Lewis and J.J. Estrada, An oceanic flood basalt province within the Caribbean plate, Earth Planet. Sci. Lett. 155, 221-235, 1998.

3. A.E. Bence, J.J. Papike and R.A. Ayuso, The petrology of submarine lavas from the central Caribbean: DSDP Leg 15, J. Geophys. Res. 80, 4775-4804, 1975.

4. A.C. Kerr, J. Tarney, G.F. Marriner, G.T. Klaver, A.D. Saunders and M.F. Thirlwall, The geochemistry and petrogenesis of the late-Cretaceous picrites and basalts of Curaçao, Netherlands Antilles: a remnant of an oceanic plateau, Contr. Min. Petrol. 124, 29-43, 1996.

5. A.C. Kerr, G.F. Marriner, J. Tarney, A. Nivia, A.D. Saunders, M.F. Thirlwall and C.W. Sinton, Cretaceous basaltic terranes in western Colombia: Elemental, chronological and

Sr-Nd constraints on petrogenesis, J. of Petrol. 38, 677-702, 1997.

6. B.G. Aitken and L.M. Echeverría, Petrology and geochemistry of komatiites and tholeiites from Gorgona island, Colombia, Contr. Min. Petrol. 86, 94-105, 1984.

7. R.J. Walker, M. Storey, A.C. Kerr, J. Tarney and N.T. Arndt, Implications of 187 Os heterogeneities in a mantle plume: Evidence from Gorgona Island and Curaçao, Geochim. Cosmochim. Acta 63, 713-728, 1999.

8. L.M. Echeverría, Tertiary or Mesozoic komatiites from Gorgona island, Colombia: Field relations and geochemistry, Contr. Min. Petrol. 73, 253-266, 1980.

9. A.C. Kerr, G.F. Marriner, N.T. Arndt, J. Tarney, A. Niva, A.D. Saunders and R.A. Duncan, The petrogenesis of Gorgona komatiites, picrites and basalts: new field, petrographic and geochemical constraints, Lithos 37, 245-260, 1996.

10. B. Dupré and L.M. Echeverría, Pb isotopes of Gorgona island (Colombia): Isotop variations correlated with magma type, Earth Planet. Sci. Lett. 67, 186-190, 1984.

11. R.J. Walker, L.M. Echeverría, S.B. Shirey and M.F. Horan, Re-Os isotopic constraints on the origin of volcanic rocks, Gorgona island, Colombia: Os isotopic evidence for acient heterogeneties in the mantle, Contr. Min. Petrol. 107, 150-162, 1991.

12. N.T. Arndt, A.C. Kerr and J. Tarney, Dynamic melting in plume heads: the formation of Gorgona komatiites and basalts, Earth Planet. Sci. Lett. 146, 289-301, 1997.

13. F. Hauff, K. Hoernle, H.-U. Schmincke and R. Werner, A Mid Cretaceous Origin for the Galápagos Hotspot: Volcanological, Petrological, and Geochemical Evidence from Costa Rican Oceanic Crustal Segments, Geol. Rdsch. 86, 141-155, 1997.

14. C.W. Sinton, R.A. Duncan and P. Denyer, Nicoya Peninsula, Costa Rica: a single suite of Caribbean oceanic plateau magmas, J. Geophys. Res. 102, 15507-15520, 1997.

15. H.-J. Gursky, The oldest sedimentary rocks of South Central America: The radiolarian cherts of the Nicoya Ophiolite Complex (?Early Jurassic to Late Cretaceous), Profil 7, 265-277, 1994.

16. J.Z. De Boer, M.S. Drummond, M.J. Bordelon, M.J. Defant, H. Bellon and R.C. Mauri, Cenozoic magmatic phases of the Costa Rican island arc (Cordillera de Talamanca), in: Geologic and Tectonic Development of the Caribbean Plate Boundary in Southern Central America, P.Mann, ed. 295, pp. 35-55, 1995.

2. Additional Literature Data

· L.M. Echeverría and B.G. Aitken, Pyroclastic rocks: Another manifestation of ultramafic volcanism on Gorgona Island, Colombia, Contr. Min. Petrol. 92, 428-436, 1986.

· K.P. Jochum, N.T. Arndt and A.W. Hofmann, Nb-Th-La in komatiites and basalts: constraints on komatiite petrogenesis and mantle evolution, Earth Planet. Sci. Lett. 107, 272-289, 1991.

· G. Sen, R. Hickey-Vargas, D.G. Waggoner and F. Maurasse, Geochemistry of basalts from the Dumisseau Formation, southern Haiti: implications for the origin of the Caribbean Sea crust, Earth Planet. Sci. Lett. 87, 423-437, 1988.

· C. H. Langmuir, East Pacific Rise Data Synthesis, in: Section IX Petrology Database, Vol. 2 and 3, Tighe S. (ed), JOI, Inc. (publ), Washington, D.C., 1988.